Electrical conductivity anisotropy of dry and hydrous olivine at 8GPa

Brent T. Poe, Claudia Romano, Fabrizio Nestola, Joseph R. Smyth

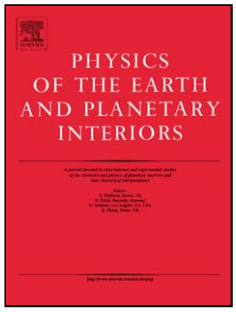

Title: Electrical conductivity anisotropy of dry and hydrous olivine at 8 GPa

Authors: Brent T. Poe, Claudia Romano, Fabrizio Nestola, Joseph R. Smyth

PII: S0031-9201(10)00102-0
DOI: doi:10.1016/j.pepi.2010.05.003
Reference: PEPI 5286

To appear in: *Physics of the Earth and Planetary Interiors*

Received date: 10-12-2009
Revised date: 3-5-2010
Accepted date: 18-5-2010

Please cite this article as: Poe, B.T., Romano, C., Nestola, F., Smyth, J.R., Electrical conductivity anisotropy of dry and hydrous olivine at 8 GPa, *Physics of the Earth and Planetary Interiors* (2008), doi:10.1016/j.pepi.2010.05.003

Electrical conductivity anisotropy of dry and hydrous olivine at 8 GPa

Brent T. Poe[a,b,*], Claudia Romano[c], Fabrizio Nestola[d], Joseph R. Smyth[e]

a. Dipartimento di Geotecnologie per l'Ambiente ed il Territorio, Università degli Studi "G. d'Annunzio" – Chieti, Via dei Vestini 30, 66013 Chieti Scalo, Italy (Tel. +39-0871-3556150, Fax +39-0871-3556047, email: poe@ingv.it)

b. Istituto Nazionale di Geofisica e Vulcanologia, Rome, Italy

c. Dipartimento di Scienze Geologiche, Universita' degli Studi di Roma Tre, Largo San Leonardo Murialdo, 1, 00146 Rome, Italy (Tel. +39-06-53778018, email: romano@uniroma3.it)

d. Dipartimento di Geoscienze, Università degli Studi di Padova, Via Giotto 1, 35137 Padova, Italy (Tel. +39-049-827-2009, email: Fabrizio.Nestola@unipd.it)

e. Department of Geological Sciences, University of Colorado, Boulder, CO 80309, USA (Tel. +001-303 492 5521, email: smyth@colorado.edu)

*Corresponding author

ABSTRACT

The effects of dissolved H_2O on the electrical conductivity and its anisotropy in olivine (Fo_{90}) at 8 GPa were investigated by complex impedance spectroscopy. At nominally anhydrous conditions, conduction along [100] and [001] is slightly higher than along [010] in contrast to observations made at lower pressures in earlier studies. Increasing H_2O content increases conductivities but activation energies are lower and H_2O concentration dependent. The use of polarized FTIR spectroscopy to determine H_2O concentrations reveals a weaker than expected effect that water has on olivine conductivity and distinguishes our results from earlier studies based on analyses using non-polarized infrared spectroscopy. We show that at H_2O concentrations of a few hundred wt ppm or less, that the dominant conduction mechanism at mantle temperatures continues via small polarons, such as that observed for anhydrous olivine. Our results also suggest that at depths greater than 200 km, the presence of H_2O may not be necessary to explain regions in the upper mantle where both electrical and seismic anisotropy are observed. This can be explained by differences in the pressure dependence of the activation energy for conduction along each of the three crystallographic axes. However, while electrical anisotropy of anhydrous olivine remains weak at 8 GPa, it is nevertheless enhanced by elevated concentrations (> several hundred wt ppm) of dissolved H_2O. At these conditions dominated by proton hopping, conductivity along [010] is highest, approximately an order of magnitude greater than along [100]. Additionally, at 1000 wt ppm and 1500°C, an isotropic conductivity derived from the data is about 1 order of magnitude higher than that for nominally anhydrous olivine. Thus, in regions of the mantle characterized by anomalously high conductivities and both electrical and seismic anisotropy, significant amounts of dissolved hydrogen can be expected.

42

43 Keywords: Electrical conductivity, high pressure, hydrous olivine, anisotropy

44

1. INTRODUCTION.

Recent studies have indicated that regions of electrical anisotropy in the mantle are highly correlated to seismic anisotropy (Simpson, 2002; Eaton et al., 2004; Evans et al., 2005) implying that knowledge of the electrical properties of olivine could provide important insights regarding mantle flow. Lattice preferred orientation (LPO) of olivine due to strain-induced deformation might account for observed electrical anisotropy at depths beginning near 60 km depth in the oceanic mantle (Evans et al., 2005) and at depths greater than 150 km below the North Central craton of Australia (Simpson, 2002). These observations lead to the suggestion that electrical conductivity in mantle olivine must be highest parallel to the [100] direction. Schock et al. (1989) and Yoshino et al. (2006) showed for single crystal olivine at 1 atm and 3 GPa, respectively, that at upper mantle temperatures electrical conduction along the [100] direction is slower than its other two principal crystallographic axes. However, in order to reconcile the simultaneous presence of both electrical and seismic anisotropy, conduction along [100] should be fast and parallel to the polarization direction of S-waves.

Laboratory data from Schock et al. (1989) and related models describing olivine conductivity (Shankland and Duba, 1990; Constable et al., 1992) are also too resistive to arrive at conductivities expected from models of magnetotelluric data corresponding to the upper mantle (Gatzemeier and Moorkamp, 2005). Constable (2006) derived a more recent model for dry olivine conduction which improves the agreement between dry olivine conductivity and the upper mantle, particularly at temperatures above 1300°C. Nevertheless, the presence of H_2O in the mantle could possibly reconcile any remaining differences between laboratory conductivity data of nominally anhydrous minerals and EM profiles generated from magnetotelluric observations. Hydrogen diffusion in olivine is faster than the mobility of intrinsic defects (Kohlstedt and

Mackwell, 1998), such that estimated conductivities of hydrous olivine through a proton conduction mechanism are in better accord with upper mantle conductivity (Karato, 1990) and electrical anisotropy (Evans et al., 2005). Wang et al. (2006) measured hydrous polycrystalline olivine conductivity at 4 GPa and concluded that 80 wt ppm H_2O in olivine would increase its conductivity by more than a factor of ten at 1400°C and account for the generally high conductivity of the oceanic asthenosphere. In contrast, Yoshino et al. (2006) concluded that extrapolation of their data to higher temperatures does not increase conductivity enough to explain the observed bulk conductivity of the upper mantle. Yoshino et al. (2006), however, did not determine how conductivity varies with varying water content along any of the three crystallographic directions, but rather assumed that conductivity increased linearly with H_2O concentration without change in activation energy. In a later study, Yoshino et al. (2009) carried out additional experiments on hydrous polycrystalline aggregates of olivine and determined the H_2O concentration dependence.

In this study, we investigate the electrical properties of single crystal San Carlos olivine (Fo_{90}) as a function of dissolved H_2O content at 8 GPa using complex impedance spectroscopy in a multianvil apparatus. We find that the higher pressure of this study has a profound influence on electrical anisotropy compared to studies at lower pressure, particularly for the case of hydrous olivine. We also find that significantly greater concentrations of H_2O in olivine (ca. 1000 ppm) are required to increase olivine conductivity by a factor of ten at upper mantle temperatures. In order to couple the conductivity data with the elastic properties of olivine we have also investigated *in situ* at high-pressure an anhydrous synthetic forsterite by single-crystal X-ray diffraction using a diamond anvil cell.

2. EXPERIMENTAL METHODS

2.1 Hydration of olivine single crystals.

Oriented single crystals of San Carlos olivine (Fo_{90}) were machined into 1.8 mm dia. x 2 mm cylinders and placed in welded Pt capsules (2.0 mm o.d.) sandwiched between a mixture of fine-grained synthetic talc ($Mg_3Si_4O_{10}(OH)_2$) and brucite ($Mg_3(OH)_6$) (weight ratio 1.4:1). Hydration runs were carried out in a multianvil apparatus at pressures ranging from 3 to 8 GPa and T=1100°C for up to 5 hours. Recovered single crystals were then cut and polished into disc-shaped specimens (0.3 - 0.6 mm thick) for complex impedance spectroscopy.

2.2 Complex impedance spectroscopy.

Complex impedances were measured at 8 GPa in either a 1000-tonne or 1200-tonne Kawai-type multianvil apparatus using 11 mm truncation edge length tungsten carbide anvils and 18 mm edge length MgO octahedra. The design of the conductivity cell is described in detail by Poe and Xu (1999). The presence of a cylindrical Mo foil shield lined with a small amount of MoO_2 powder is a key component of the cell. The shield is placed between sample and furnace primarily to minimize interference between the higher 50 Hz voltage applied to operate the furnace and the variable frequency signal applied across the electrodes to measure complex impedance. Additionally, the shield is grounded in common with the furnace to eliminate current leakage along the outer surface of the sample and also serves as a fO_2 buffer according to the $Mo + O_2 = MoO_2$ equilibrium. Both Wang et al. (2006) and Yoshino et al. (2006) used Ni / NiO to buffer their lower pressure experiments, whereas Yoshino et al. (2009) also used Mo /MoO2 to buffer their 10 GPa experiments. Measurements were made with a Solartron 1260 Impedance/Gainphase analyzer operating at 1.0 V amplitude and frequencies from 10^5

to 10^{-1} Hz. A typical measurement consisted of heating to a maximum temperature, depending on volatile content, and repeatedly acquiring the complex impedance spectrum every 10 to 15 minutes until it remained unchanged (on the order of 1 hour). Subsequent spectra were taken upon decreasing temperature only in order to maintain the sample's H_2O concentration (measured post-run) in light of possible dehydration at the maximum temperature of the measurement. It is quite likely that for the more H_2O-rich samples, partial dehydration occurred at the maximum temperature (Yoshino et al., 2006). However, afterwards, at lower temperatures, observed Arrhenian behavior would suggest a negligible amount of additional dehydration. The complex impedance data were fit to an expression for an RC parallel equivalent circuit, allowing for some deviation (< 10°) of the circle center from the real axis. From the determined resistance and the sample and electrode dimensions, electrical conductivity was determined. Experimental error, arising mainly from uncertainties in the sample dimensions and any non-ideality of the form of the data with respect to the equivalent circuit, is estimated to be about 5% relative.

2.3 Polarized FTIR spectroscopy.

Samples recovered after complex impedance spectroscopy were analyzed by polarized infrared spectroscopy using a Bruker IFS 120 HR high resolution Fourier-transform spectrometer and IR microscope with Cassegranian optics. The concentration of dissolved H_2O in olivine was determined using the calibration of Bell et al., (2003) who showed that the calibration of Paterson (1982) for unpolarized FTIR spectra may underestimate water content in olivine by a factor of 2-4 owing to the extreme IR pleochroism of olivine. Table 1 lists H_2O concentrations (in wt ppm) for samples after complex impedance measurements. Similar to previous observations (Mosenfelder et al., 2006; Smyth et al., 2006; Kohlstedt et al., 1996) for laboratory-synthesized H_2O-

144 rich samples, multiple absorption bands in the range 3300-3500 cm^{-1} are observed in
145 addition to the main peaks between 3500 and 3600 cm^{-1}.

146 *2.4 Single crystal XRD.*

147 In order to better understand how differences in electrical conductivity might be related
148 to structural changes to the crystal lattice at these conditions, we also performed a series
149 of single crystal X-ray diffraction measurements. A colorless single crystal of pure
150 forsterite, free of twins and inclusions, was synthesized at room pressure and 1600°C.
151 Although the chemical composition of the crystal was slightly different to those of the
152 electrical measurements, we assume that the general behavior observed can be useful to
153 our interpretation of the conductivity results. The crystal, with dimensions 80×60×50
154 μm^3, was loaded in a BGI-type diamond-anvil cell (DAC) with T301 steel foil gasket. A
155 mixture of methanol:ethanol (4:1) served as pressure-transmitting medium. A quartz
156 crystal was added as an internal pressure standard (Angel et al. 1997). Unit-cell
157 parameters (Table 1) were determined at 19 different pressures up to about 6.8 GPa and
158 room temperature on a Huber four-circle diffractometer (non-monochromatized $Mo_{K\alpha}$
159 radiation) using eight-position centering of not less than 20-22 Bragg reflections
160 according to the procedure of King and Finger (1979). Centering procedures and vector-
161 least-square refinement of the unit-cell constants were performed using the SINGLE04
162 software (Angel et al. 2001) according to the protocols of Ralph and Finger (1982)
163 without any symmetry constraints in order to monitor possible high-pressure phase
164 transformations. The unit-cell parameters data at each pressure are reported in Table 1.

165 3. RESULTS AND DISCUSSION

166 *3.1 Hydrogen incorporation in olivine*.

The solubility of hydrogen in olivine is low compared to its higher pressure polymorphs wadsleyite and ringwoodite (Kohlstedt et al., 1998). However, recent studies that utilized polarized FTIR spectroscopy have shown that H_2O solubility in olivine is higher by as much or more than a factor of two compared to previous studies that used non-polarized FTIR spectroscopy (Bell et al., 2003; Mosenfelder et al., 2006). An example of our polarized FTIR spectra is shown in Fig. 1 for the H_2O-rich sample S3740. Absorption is strongest with the electric field gradient, E, oriented parallel to the *a*-axis, consistent with the observations of previous studies (Kohlstedt et al., 1998; Bell et al., 2003; Mosenfelder et al., 2006). Also, similar to Kohlstedt et al. (1998) we observe several strong absorption bands at lower OH stretching frequencies (3300-3500 cm^{-1}) in our synthetically hydrated samples which do not appear in the spectra of natural olivine samples having much lower H_2O concentrations (Mosenfelder et al., 2006). Differences between the spectra of synthetically hydrated and natural olivine specimens illustrate that hydrogen incorporation in olivine is a complex function of oxygen fugacity and silica activity in addition to water fugacity (Mosenfelder et al., 2006). The pressure of the hydration experiments varied from 3 to 8 GPa in order to vary water fugacity and resulted in a range of H_2O concentrations from 363 to 2215 wt ppm (see Table 1), based on the calibration of Bell et al. (2003) for polarized FTIR spectra. Interestingly, in earlier attempts to hydrate single crystals of olivine using a piston cylinder apparatus (up to 3 GPa) the recovered run products were often opaque and/or fractured such they could not be used for conductivity measurements. Uncertainties in the effect of H_2O on conductivity are primarily related to these analyses, however, as spectra could be obtained only post electrical measurement in order to preserve sample geometry and orientation for determination of its conductivity. Additional sources of error in the H_2O concentrations stem from inhomogeneities revealed upon reducing the

size of the aperture (< ca. 600 μm^2) and uncertainties in baseline subtraction owing to spectra composed of very broad and overlapping absorption bands.

3.2 Complex impedance spectra.

A representative suite of complex impedance spectra for a hydrated single crystal of olivine oriented along its (100) axis (H2474) is shown in Fig. 2. Each spectrum is characterized by a semi-circular pattern of data spanning from the axes origin at the highest frequencies, reaching a minimum imaginary component (Z″) and returning toward the abscissa with increasing real impedance (Z′) at very low frequencies. With increasing temperature, the shape of the spectrum remains semi-circular and its diameter, which is proportional to the sample's electrical resistance, decreases. We note that with decreasing frequency, particularly at lower temperatures (see Fig. 2), the scatter in the data markedly increases, most likely due to increasingly higher impedances. While it has been assumed in several previously published studies that the measured impedance at a single frequency, provided that the frequency is sufficiently low, may be equal to the sample resistance (Schock et al., 1989; Fu-jita et al., 2004, Yoshino et al., 2008), such an assumption in our case would lead to large uncertainties. Over the experimental spectral range, spanning 6 decades in frequency, a majority of the semicircular arc is observed, providing a lower uncertainty of the sample resistance compared to any single low frequency measurement.

Conductivities are shown for each crystallographic direction at anhydrous and various concentrations of dissolved H_2O in Fig. 3. For each individual sample log conductivity decreases linearly with reciprocal temperature according to the Arrhenius expression

$$\sigma = \sigma_0 \exp(-H/kT) \qquad \text{Eq. 1}$$

where k is the Boltzmann constant, T the absolute temperature and log σ_0 and H the intercept and slope, respectively, of the linear regressions. Best fit values of the pre-exponential term σ_0 and the activation enthalpy H for each experiment are listed in Table 2 along with crystallographic orientation and measured H_2O concentration. Because the correlation of the data to Eq. 1 is very high in all cases, we have assumed that H_2O concentration during the electrical measurement remained constant and equal to that of the post-measurement FTIR analysis of the sample. Although it is not observed here, non-Arrhenian behavior would likely be the result of either a change in chemical composition during the measurement, such as loss of dissolved H_2O, or from a temperature dependent change in the conductivity mechanism. In the former case, such behavior would be irreversible with temperature, whereas in the latter case, we can expect the behavior to be reversible and characterized by a stronger temperature dependence (higher H) at lower 1/T.

3.3 Electrical conductivity of dry olivine.

For the anhydrous samples, conductivities were determined at temperatures ranging from 850 to 1436°C, overlapping both the small polaron and Mg vacancy conduction regimes expected as the dominant charge transport mechanisms at low and high temperatures, respectively at 1 atm (Schock et al., 1989; Hirsch et al., 1993; Constable and Roberts, 1997; Dufrane et al., 2005). Also shown in Fig. 3 are the results of Yoshino et al. (2006) obtained at 3 GPa, in very good agreement with our data for anhydrous olivine. Given that our measurements were carried out at 8 GPa, the agreement among our data and those of Yoshino et al. (2006) strongly reflects the low activation volume (< 1 cm^3/mol) for electrical conduction of olivine determined by Xu et al. (2000). A low activation volume also supports the notion that the conduction mechanism is electronic, such as via small polarons which involves the hopping of

electron holes. In contrast, an ionic conduction mechanism involving the hopping of ionic species and vacancies, would require lattice distortions resulting in highly positive activation volumes on the order of several cm^3/mol (Keyes, 1963; Samara, 1984). The absence of a second conduction mechanism which would otherwise be indicated by a break in slope in the data shown in Fig. 3 (open red triangles) suggests that the conductivity is governed predominantly through small polarons, even at temperatures as high as 1436°C. We note that Yoshino et al. (2009) did observe ionic conduction in their dry polycrystalline olivine at 10 GPa. However, they report that small polaron conduction continues up to 1477°C, with ionic conduction taking over at higher temperatures up to their maximum T=1727°C.

The lower pressure studies of both Shock et al. (1989) and Yoshino et al. (2006) indicate that conduction along [100] is lower compared to one or both of the other crystallographic directions. Despite the seemingly good agreement illustrated in Fig. 3 between our data and those of Yoshino et al. (2006) at anhydrous conditions, at 8 GPa and 1200°C we find that conduction along [100] and [001] are about equal and approximately 0.2 log units higher compared to [010]. This difference can be attributed to the small, but distinct changes in activation enthalpy from 3 to 8 GPa along each crystallographic axis. While the activation enthalpy for conduction along [100] remains high, it is reduced along both [010] and [001] in comparison to those at 3 GPa reported by Yoshino et al. (2006). A reduction in activation enthalpy with increasing pressure, here for the case of small polaron conduction, can be explained by decreasing interatomic distances between Fe^{2+} and Fe^{3+}, which facilitate the electron hole hopping mechanism.

Results from our single crystal diffraction measurements of forsterite up to 6.7 GPa indicate that the [100] direction is the least compressible of the three axes, in good

agreement with other recent in-situ single crystal x-ray diffraction studies (Liu and Lee, 2006; Katsura et al., 2009) and with resonant ultrasonic spectroscopy (Isaak et al., 1989). At high pressure, interatomic distances would thus be shortened more along both the *b* and *c* directions compared to the *a* direction (Fig. 4). A more rapidly changing cell parameter is likely to be accompanied by a greater change in activation energy for conduction in that direction. Thus, at 8 GPa and the higher temperatures associated with the deeper upper mantle, conductivity along [100] becomes higher than [010], opposite to that which is observed at ambient pressure (Schock et al., 1989) and at 3 GPa (Yoshino et al., 2006).

For dry olivine conductivity anisotropy remains relatively weak because of the minor changes in temperature dependence from 3 to 8 GPa. However, the higher conductivity along [100] presents important implications where both electrical and seismic anisotropy are observed in the upper mantle. Because both high conductivities and fast shear wave velocities cannot be rationalized by LPO in dry olivine at shallow depths (≤ 3 GPa), the presence of dissolved H_2O in olivine has been suggested as responsible for favoring conduction along [100] via a fast proton conduction mechanism (Evans et al., 2005). Based on our data at 8 GPa corresponding to greater depths (> 200 km), proton diffusion is not required to justify a higher conductivity along [100] and the observed electrical anisotropy at these depths, such as below the North Central craton of Australia (Simpson, 2002). Because the effects of pressure and temperature on the electrical conductivity of dry olivine are different along each crystallographic direction, electrical anisotropy changes with depth in the mantle without requiring the presence of dissolved hydrogen to invoke a different conduction mechanism. The absence of an ionic conduction pathway at 8 GPa may also contribute to the difference in anisotropy that is observed at 3 GPa (Yoshino et al., 2006). We also stress that this conclusion can be

drawn independently of our conductivity results for hydrous olivine which are discussed below (Section 3.4), and therefore is not compromised by the additional experimental uncertainties due to analyses of H_2O content nor by long extrapolations of those data to the higher temperatures associated with the mantle.

If we apply the geometric mean of the three data sets to generate an isotropic model for dry olivine conductivity, we find that at 8 GPa and 1200°C conductivity is 2.97×10^{-3} S/m, in very close agreement with the geometric mean of 2.14×10^{-3} S/m at the same temperature calculated using the results of Yoshino et al. (2006) at 3 GPa and a value of 2.02×10^{-3} S/m at 10 GPa using the results of Yoshino et al. (2009). Both of these values compare well to mantle conductivity values below the Canadian shield (Neal et al., 2000) and below the French Alps (Tarits et al., 2004) using a standard geotherm to extract a comparative temperature from the MT profiles. These values, however, are low in comparison to the oceanic mantle at the same temperature (Evans et al., 2005). Thus, while our data for dry olivine at 8 GPa may reconcile both electrical and seismic anisotropy at deep continental mantle depths, we must still explore the effect of water on electrical anisotropy where there may be poor agreement in the absolute electrical conductivity.

3.4 Hydrous olivine conductivity.

For the hydrous olivine samples, temperatures did not exceed 700°C during the measurement in order to minimize possible dehydration of the sample. We can not exclude the possibility that the dominant conduction mechanism in hydrous olivine changes at temperatures above 700°C. However, Wang et al (2006) measured the conductivity of polycrystalline hydrous olivine at temperatures as high as 1000°C and determined an activation enthalpy of 87 kJ/mol (ca. 0.9 eV), significantly lower than

that for dry olivine conduction and similar to the activation enthalpies observed in this study at lower H_2O concentrations (see Table 2).

In Fig. 3 we see that the effect of dissolved H_2O in olivine is to increase its conductivity while decreasing its activation energy. Thus, the effect of H_2O on conductivity diminishes with increasing temperature. Yoshino et al. (2006) measured only one hydrous olivine sample for each crystallographic direction, and thus would not have been able to recognize this trend if it were present at 3 GPa. Yoshino et al. (2009), however, did observe this behavior in their later study of polycrystalline olivine at 10 GPa and also for conductivities of hydrous wadsleyite and hydrous ringwoodite (Yoshino et al., 2008), which are high pressure polymorphs of olivine. They suggested that increasing H_2O content in these phases resulted in behavior similar to that of N-type semiconductors, according to the equation

$$\sigma = \sigma_0 C_W \exp\left(-\frac{H - \alpha C_W^{1/3}}{kT}\right) \qquad \text{(Eq. 2)}$$

In the case of hydrous olivine, Yoshino et al. (2006), Wang et al (2006) and Yoshino et al. (2009) also determined their H_2O concentrations using FTIR spectroscopy, but all according to the calibration of Paterson (1982) for non-polarized spectra. Our H_2O determinations are based on the calibration of polarized FTIR spectra by Bell et al. (2003), who demonstrated its importance for pleochroic minerals. Mosenfelder et al. (2006) recently pointed out that use of the Paterson calibration for determining dissolved H_2O concentrations in Fe-bearing olivine can underestimate concentrations by as much as a factor of 4 compared to its determination by the calibration of Bell et al. (2003). The use of a different FTIR calibration may contribute to the differences in the effect of dissolved H_2O on the conductivity of olivine in our study compared to the study of Yoshino et al. (2006). If the H_2O concentrations from Yoshino et al. (2006)

were underestimated due to their use of the Paterson calibration, then the effect of dissolved H_2O on olivine conductivity that they report would be overestimated by a similar factor.

We have chosen to fit the hydrous olivine data separately from the anhydrous data based on two observations upon examination of Fig. 3 and Table 2. Most importantly, individual datasets show strongly Arrhenian behavior, which allows us to assume that a single charge transport process dominates each sample's electrical conductivity. Slight changes in slope are detectable only in the case of conduction along [100] at the lowest H_2O concentration and along [001] at the highest H_2O concentration (Fig. 3). Because we do not observe any systematic occurrence, rather than indicating a change in conduction mechanism, this behavior may be related to some form of experimental factor, such as insufficient time allowed for sample re-equilibration at lower temperatures. Secondly, activation enthalpies are clearly lower and most likely H_2O concentration dependent for the hydrous olivine data. This latter observation suggests that the dominant mechanism in hydrous olivine can not be the same as that for anhydrous olivine.

Our fits of Eq. 2 to the hydrous olivine conductivity data for each of the three crystallographic orientations are also illustrated in Fig. 3. We note that within experimental error, these H_2O concentration dependent approximations are in excellent agreement with the simple Arrhenian fits to each individual dataset. Best fit parameters are listed in Table 3. Also shown in Fig. 3 are the approximations reported by Yoshino et al. (2006) for dry and [H_2O]-independent hydrous olivine conductivity. We can compare our results to those for hydrous, polycrystalline olivine (Yoshino et al., 2009) and its higher pressure polymorphs wadsleyite and ringwoodite (Yoshino et al., 2008) in which the same form of Eq. 2 was used (note that both Yoshino et al. 2008 and 2009

use concentration units of wt% rather than wt ppm and we convert their values of σ_o and α accordingly for comparison below). Our best fit values for σ_o range from ca. 0.001 S/m along [100] to 0.3 S/m along [010]. These values are in excellent agreement with that for the proton conduction term from Yoshino et al. (2009), $\sigma_o = 0.0079$, as well as their study of hydrous wadsleyite and ringwoodite, with $\sigma_o = 0.008$ and 0.0028 S/m, respectively (Yoshino et al., 2008). The best fit values of H from Eq. 2 range from 0.8 eV along [001] to 1.5 eV along [010], in good agreement with 0.92 eV for polycrystalline olivine from Yoshino et al. (2009) and the values of 0.7 and 1.1 eV for wadsleyite and ringwoodite, respectively (Yoshino et al., 2008). Finally, the H_2O-concentration dependence parameter, α, ranges from 0.03 to ca. 0.07, which, according to Eq. 2 results in a progressively shallower slope of log σ vs. 1/T with increasing H_2O content. The values of α from Yoshino et al. (2009) for olivine and from Yoshino et al. (2008) for wadsleyite and ringwoodite range between $9x10^{-4}$ to 0.03.

We also fit the equation used by Wang et al (2006) to our data for hydrous olivine. The form of the equation and results from those fits are also given in Table 3. Similar to Eq. 2, the pre-exponential term is concentration dependent, but includes two adjustable parameters, σ_o and r. Here we find that the σ_o term returns a very large relative error. Additionally, the higher χ^2 values from this fit compared to the fit using Eq. 2 are the result of a fixed rather than H_2O concentration dependent activation enthalpy, even though the total number of adjustable parameters is the same for both fits. Interestingly, the best fit values for the exponent r (from about 2.5 along [100] to 3.5 along [010] and [001]) are much higher than that determined by Wang et al (2006) for hydrous polycrystalline olivine (ca. 0.6). As Wang et al. (2006) discussed, the value of r is indicative of the type of defect mechanism that controls proton hopping. Romano et al (2009) measured the electrical conductivity of hydrous wadsleyite and determined a

388 best-fit value of r = 1.44 using the same equation. As stated previously, the higher
389 temperature measurements of Wang et al (2006) may explain some of the differences
390 from our study as the mechanism for conduction may change with increasing
391 temperature. Indeed, Wang et al. (2006) assumed that both small polaron and proton
392 hopping conduction mechanisms contributed to the bulk conductivity at high
393 temperature, such that the fits to their data included both a dry (small polaron)
394 component and a wet (proton hopping) component. However, it is clear that at lower
395 temperatures, the temperature dependence for conductivity is strongly coupled to
396 dissolved water content in olivine such that Eq. 2 provides a much more robust
397 approximation of the experimental data.

398 *3.5 Important differences from previous studies.* A comparison of our results to those
399 from Wang et al. (2006) and Yoshino et al. (2006) is made difficult because of the
400 pressure effects that are likely to play a role between 3 or 4 GPa and 8 GPa. Regardless
401 of such effects, however, neither Wang et al. (2006) nor Yoshino et al. (2006)
402 demonstrate any link between temperature dependence of conductivity and H_2O
403 concentration. Our results show that activation enthalpy decreases with increasing water
404 concentration. This observation not only indicates that the proton hopping mechanism
405 becomes less important at higher temperatures as small polaron conduction begins to
406 dominate, but also that the effect of dissolved water diminishes with increasing
407 temperature. Yoshino et al. (2009) later investigated the effect of water concentration at
408 10 GPa, but on polycrystalline olivine aggregates. Their study, like ours, observes small
409 polaron conduction to temperatures above 1700 K in nominally anhydrous samples.
410 Similar to our results, Yoshino et al. (2009) show that activation enthalpy decreases
411 with increasing H_2O content, but their dependence (α term, Table 3) is less than what is
412 observed here. The reason for this difference is still unclear as the pressures and

temperatures of both studies are quite similar. The major differences in the experimental approach are that Yoshino et al. (2009) used polycrystalline samples, non-polarized FTIR spectroscopy and a corresponding FTIR calibration by Paterson (1982) whereas our study examined single crystal samples, and determined H_2O contents using polarized FTIR and calibration by Bell et al. (2003).

The fit to Eq. 2 allows us to determine electrical anisotropy, given simply by the difference between log σ_{max} and log σ_{min} among the three different crystallographic directions as a function of temperature, shown for nominally anhydrous olivine and at H_2O concentrations of 100 and 1000 wt ppm in Fig. 5. We can justify extrapolation of the hydrous data to higher temperatures as the conductivities remain higher than those for dry olivine, except in the case of [001] above 1350°C at the lowest H_2O concentration (see Fig. 3). No extrapolations are made for dry olivine for which electrical anisotropy is determined using the fit parameters to the Arrhenius expression (Table 2). For both anhydrous olivine and at 100 ppm wt H_2O, conduction along [100] remains highest. Interestingly, at 100 wt ppm H_2O, electrical conductivity is more isotropic than that of dry olivine. However, at 1000 wt ppm H_2O, electrical anisotropy is greater, by about a factor of ten along [010] compared to the [001] direction. At these H_2O rich conditions, anisotropy is nearly independent of temperature. The complex behavior we observe over this range of H_2O content could be related to the speciation of H_2O in olivine as a function of its concentration, which is still poorly understood at present. Hushur et al. (2009) report that the high pressure hydration mechanism in forsterite is principally M1 site vacancy with the proton on the O1-O2 edge shared between M1 octahedra. This mechanism would increase *c*-axis compressibility and facilitate proton movement along the edge-sharing M1 octahedral chains parallel to *c*. We would then expect a lower activation enthalpy along *c* compared to *b* for conduction

dominated by proton hopping (see Table 3) much like what we observe for the anhydrous case of small polaron hopping where *b*-axis compressibility is greatest (Fig. 4) and its activation enthalpy lowest (Table 2). This would of course influence its anisotropy but in a different manner compared to anhydrous olivine or H_2O-poor olivine for which the dominant conduction mechanism may be unrelated to the presence of hydrogen (see below Section 3.6).

3.6 Competing charge transport mechanisms.

It is important to note that the anhydrous data are not included in the fit to Eq. 2 because the conduction process cannot involve a protonated charge carrier. Even at low H_2O concentrations, the activation enthalpy is lower than that for anhydrous olivine, such that at higher temperatures it would be expected to intersect the anhydrous data. This suggests that electrical conduction in hydrous olivine is dominated by a proton-bearing charge carrier at low temperatures but crosses over to the small polaron conduction mechanism at a temperature that depends on the H_2O concentration. By combining the results of the fits to Eq. 2 for hydrous olivine with the best fit parameters to the Arrhenius equation for the anhydrous data, we can determine the temperature of this crossover for the total geometric mean electrical conductivity, which is equal to the sum of the small polaron (σ_{Fe}) and proton (σ_H) geometric mean conductivities

$$\sigma = \left(\sigma_{Fe100} \cdot \sigma_{Fe010} \cdot \sigma_{Fe001}\right)^{\frac{1}{3}} + \left(\sigma_{H100} \cdot \sigma_{H010} \cdot \sigma_{H001}\right)^{\frac{1}{3}} \quad \text{Eq. 3}$$

Figure 6a illustrates the variation of log σ with H_2O concentration and temperature and the boundary between the small polaron dominant and H-bearing dominant fields. The cross-over temperature indicated by the dashed black line increases smoothly with log [H_2O]. We find that the slope of the boundary is quite steep due to the large change in activation energy with increasing H_2O content. At H_2O concentrations below a few

hundred wt ppm, the dominant charge transport mechanism is that of small polarons. Fig. 6b shows similar behavior using the results of Yoshino et al. (2009). At the far left of the plot beginning at 10 wt ppm H_2O, which corresponds to small polaron conduction, the two models are in very good agreement. Only at the highest temperatures, at which Yoshino et al. (2009) observe ionic conduction, do the nominally anhydrous conductivities begin to diverge. For hydrous olivine, our results show that the strong H_2O concentration dependence of the cross-over temperature implies that significant concentrations of dissolved H_2O (several hundred wt ppm) could cause the mantle to switch from small polaron to proton hopping conduction. The results from Yoshino et al. (2009), however, would indicate this to be less likely due to a weaker H_2O concentration dependence. We have assumed that the effect of H_2O on the small polaron mechanism has a negligible effect on the anhydrous conductivity simply because we have no conductivity data for hydrous olivine at sufficiently high temperatures that might be suggestive of a different conduction mechanism. However, it is likely that dissolved H_2O in olivine also influences the small polaron conductivity indirectly through its effect on the fO_2 via autodissociation,

$$H_2O = H_2 + ½O_2 \qquad \text{Eq. 4}$$

and how the change in oxidation state influences the ratio of ferric to ferrous iron. Thus, the effect is likely to be slightly positive, and therefore the boundaries shown in Fig. 6 would represent the minimum temperature of the crossover.

3.6 Conclusions.

As mentioned above, with increasing temperature the effect of H_2O concentration diminishes. However at 1500°C, the calculated isotropic conductivity (geometric mean) at 1000 ppm H_2O remains a factor of ten higher than that for nominally anhydrous

olivine. We conclude that in the deeper half of the upper mantle, both the absolute conductivity and electrical anisotropy of H_2O-bearing olivine can indeed account for observed magnetotelluric signatures which result in either anomalously high conductivities or strong anisotropy associated with similar anomalously high shear velocities. In other words, in the deeper regions of the upper mantle where both the absolute conductivity and electrical anisotropy are anomalously high, we cannot rule out the possibility that high concentrations of dissolved H_2O (several hundred wt ppm or more) in olivine may be present.

We must also note that variations in both silica and oxygen activities play important roles on the electrical properties of olivine (Wanamaker and Duba, 1993; Du Frane et al., 2005). Although we have not addressed these chemical parameters in our study, it is clear that small changes in H_2O concentration still result in measureable changes in electrical conductivity. Within the dry olivine stability field, Du Frane et al. (2005) demonstrated that a difference of more than five orders of magnitude in fO_2 is required to change its conductivity by a factor of ten. Within the chemical environment defined by our experiments, conceivable lateral variations in H_2O concentration from nominally anhydrous to 0.1 wt% can achieve the same relative change.

Lastly, we emphasize that the effect of H_2O on the electrical conductivity of olivine is pressure, temperature and H_2O concentration dependent. Our results show that these effects are not as large as previously suggested, possibly due to differences in both experimental and analytical approaches. Most importantly, because the activation energy for H-bearing conduction mechanisms are significantly lower than those for electronic conduction, these effects become less important with increasing depth (i.e. increasing temperature) in the mantle. Unfortunately, this also implies that experimental studies to determine the electrical conductivity of hydrous phases stable at lower mantle

511 conditions may not necessarily be useful in constraining the water content at very deep
512 mantle depths.

513 ACKNOWLEDGEMENTS

514 We are grateful to H. Fisher and H. Schulze of the Bayerisches Geoinstitut (University
515 of Bayreuth) for technical assistance. High-pressure experiments were performed at the
516 Bayerisches Geoinstitut under the EU "Research Infrastructures: Transnational Access"
517 Programme (Contract No. 505320 (RITA) - High Pressure). We also thank two
518 anonymous reviewers for their helpful comments.

519 REFERENCES

520 Angel, R.J., D.R. Allan, R. Miletich, L.W. Finger (1997) The use of quartz as an
521 internal pressure standard in high-pressure crystallography. Journal of Applied
522 Crystallography, 30, 461-466.

523 Angel, R.J., R.T. Downs, L.W. Finger (2001) High-Temperature-High-Pressure
524 Diffractometry. In Hazen, R.M., Downs, R.T. (Eds.), High-pressure, high-temperature
525 crystal chemistry. Reviews in Mineralogy and Geochemistry, 41, 559-596.

526 Bell, D. R., G. R. Rossman, J. Maldener, D. Endisch, F. Rauch, (2003), Hydroxide in
527 olivine: a quantitative determination of the absolute amount and calibration of the IR
528 spectrum, J. Geophys. Res., 108(2105), 10.1029/2001JB000679.

529 Constable, S. (2006) SEO3: a new model of olivine electrical conductivity. Geophys. J.
530 Int. 166, 435-437.

531 Constable, S. and J. J. Roberts (1997) Simultaneous modelling of thermopower and
532 electrical conduction in olivine, Phys. Chem. Min., 24, 319-325.

533 Constable, S. C., T. J. Shankland, and A. G. Duba (1992) The electrical conductivity of
534 an isotropic olivine mantle, J. Geophys. Res., 97, 3397-3404.

535 Du Frane, W. L., J. J. Roberts, D. A. Toffelmier, and J. A. Tyburczy (2005), Anisotropy
536 of electrical conductivity in dry olivine, Geophys. Res. Lett., 32, 24315, doi:
537 10.1029/2005GL023879.

538 Eaton, D. W., A. G. Jones, and I. J. Ferguson (2004), Lithospheric anisotropy structure
539 inferred from collocated teleseismic and magnetotelluric observations: Great Slave Lake
540 shear zone, northern Canada, Geophys. Res. Lett., 31, L19614, doi:
541 10.1029/2004GL020939.

542 Evans, R. L., G. Hirth, K. Baba, D. Forsyth, A. Chave, and R. Mackie (2005),
543 Geophysical evidence from the MELT area for compositional controls on oceanic
544 plates, Nature, 437, 249-252.

545 Fu-jita, K., T. Katsura and Y. Tainosho (2004), Electrical conductivity measurement of
546 granulite under mid- to lower crustal pressare-temperature conditions. Geophys. J. Int.
547 157, 79-86.

548 Gatzemeier, A. and M. Moorkamp (2005) 3D modelling of electrical anisotropy from
549 electromagnetic array data: hypothesis testing for different upper mantle conduction
550 mechanisms, Phys. Earth Planet. Int., 149, 225-242.

551 Hirsch, L.M., Shankland, T.J., Duba, A.G., 1993. Electrical conductivity and polaron
552 mobility in Fe-bearing olivine. Geophys. J. Int. 114, 36–44.
553

554 Hushur, A., M.H. Manghnani, J. R. Smyth, F. Nestola, and D.J. Frost (2009) Crystal
555 chemistry of hydrous forsterite and its vibrational properties up to 41 GPa. Am.
556 Mineral. 94 (in press).

557 Isaak, D.G., Anderson, O.L., Goto, T. (1989). Elasticity of single crystal forsterite
558 measured to 1700 K. J. Geophys. Res. 94, 5895–5906.
559

560 Karato, S. (1990) The role of hydrogen in the electrical-conductivity of the upper
561 mantle, Nature, 347(6290), 272– 273.

562 Katsura, T., et al., (2009) Thermal expansion of forsterite at high pressures determined
563 by in situ x-ray diffraction: the adiabatic geotherm in the upper mantle. Phys. Earth
564 Planet. Int., in press.

565 Keyes, R.W., 1963. Continuum models of the effect of pressure on activated process.
566 In: Paul, W., Warschauer, D.M._Eds.., Solids Under Pressure. McGraw-Hill, New
567 York, pp. 71–99.

568 King, H.E. and L. Finger (1979) Diffracted beam crystal centering and its application to
569 high pressure crystallography. Journal of Applied Crystallography, 12, 374–378.

570 Kohlstedt, D. L. and S. J. Mackwell (1998) Diffusion of hydrogen and point defects in
571 olivine, Z. Phys. Chem., 207, 147-162.

572 Liu, W. and Lee, B. (2006) Thermal equation of state of (Mg0.9Fe0.1)2SiO4 olivine.
573 Phys. Earth Planet. Int. 157, 188-195.

574 Mosenfelder, J. L., N.I. Deligne, P. D. Asimov, G. R. Rossman (2006) Hydrogen
575 incorporation in olivine from 2-12 GPa, Amer. Mineral., 91, 285-294.

576 Neal, S. L., R. L. Mackie, J. C. Larsen, and A. Schultz (2000) Variations in the
577 electrical conductivity of the upper mantle beneath North America and the Pacific
578 Ocean. J. Geophys. Res., 105(B4), 8229-8242.

579 Paterson, M. S. (1982) The determination of hydroxyl by infrared-absorption in quartz,
580 silicate-glasses and similar materials, Bull. Mineral., 105, 20-29.

581 Ralph, R.L., L.W. Finger (1982) A computer program for refinement crystal orientation
582 matrix and lattice constants from diffractometer data with lattice symmetry constrains.
583 Journal of Applied Crystallography, 15, 537–539.

584 Romano, C., B.T. Poe, J. Tyburczy, and F. Nestola (2009) Electrical conductivity of
585 hydrous wadsleyite, Eur. J. Mineral., 21, 1615-622.

586 Samara, G.A. (1984) High-pressure studies of ionic conductivity in solids. In:
587 Ehrenreich, H., D. Turnbull, eds., Solid State Physics, Advances in Research and
588 Applications, vol. 38. Academic Press, London, pp. 1-80.

589 Schock, R.N., A.G. Duba, and T.J. Shankland (1989) Electrical conduction in olivine. J.
590 Geophys. Res., 94, 5829-5839.

591 Shankland, T.J. and A.G. Duba (1990) Standard electrical conductivity of isotropic,
592 homogeneous olivine in the temperature range 1100-1500°C. Geophys. J. Int., 103, 25-
593 31.

594 Simpson, F. (2002), Intensity and direction of lattice-preferred orientation of olivine:
595 Are electrical and seismic anisotropies of the Australian mantle reconcilable? Earth
596 Planet. Sci. Lett., 203, 535–547.

597 Smyth, J.R., D.J. Frost, F. Nestola, C.M. Holl, and G. Bromiley (2006) Olivine
598 hydration in the deep upper mantle: Effects of temperature and silica activity. Geophys.
599 Res. Lett., 33, L15301.

600 Tarits, P., S. Hautot, and F. Perrier (2004) Water in the mantle: Results from electrical
601 conductivity beneath the French Alps, Geophys. Res. Lett., 31, L06612, doi:
602 10.1029/2003GL019277.

603 Wanamaker, B. J., and A. G. Duba (1993), Electrical conductivity of San Carlos olivine
604 along [100] under oxygen- and pyroxene-buffered conditions and implications for
605 defect equilibria, J. Geophys. Res., 98, 489– 500.

606 Wang, D. J., M. Mookherjee, X. S. Xu, and S. Karato (2006) The effect of water on the
607 electrical conductivity of olivine, Nature, 443, 977-980.

608 Xu, Y., T. J. Shankland, and A. G. Duba (2000), Pressure effect on electrical
609 conductivity of mantle olivine, Phys. Earth Planet. Inter., 118, 149– 161.

610 Yoshino, T., M. Takuya, S. Yamashita, and T. Katsura (2006) Hydrous olivine unable
611 to account for conductivity anomaly at the top of the asthenosphere, Nature, 443, 973-
612 976.

613 Yoshino, T., G. Manthilake, T. Matsuzaki, and T. Katsura (2008) Dry mantle transition
614 zone inferred from the conductivity of wadsleyite and ringwoodite, Nature 451, 326-
615 329.

616 Yoshino, T., T. Matsuzaki, A. Shatskiy, and T. Katsura (2009) The effect of water on
617 the electrical conductivity of olivine aggregates and its implications for the electrical
618 structure of the upper mantle. Earth and Planetary Science Letters 288, 291-300.

619 FIGURE CAPTIONS

620 FIG. 1 Polarized FTIR spectra of a hydrous olivine single crystal with H_2O content of
621 2215 wt ppm.

622

623 FIG. 2 Representative complex impedance spectra of a hydrous olivine single crystal at
624 8 GPa and temperatures ranging from 500 to 700 °C.

625

626 FIG. 3 Electrical conductivity of olivine at 8 GPa along different crystallographic
627 directions at various concentrations of dissolved H_2O (wt ppm). Black dashed lines are
628 reproduced from Yoshino et al., 2006. Solid red lines are Arrhenian fits (Eq. 1) through
629 the data for nominally anhydrous olivine. Solid green and blue lines are fits of Eq. 2
630 through the data for hydrous olivine conductivities.

631

632 FIG. 4 Variation of forsterite lattice parameters as a function of pressure up to 6.7 GPa
633 at room temperature from single crystal x-ray diffraction.

634

635 FIG. 5 Electrical anisotropy given as the difference between log σ_{max} and log σ_{min} as a
636 function of temperature for dry, 100 ppm and 1000 ppm wt H_2O.

637

638 FIG. 6 Geometric mean electrical conductivity (see Eq. 4) as a function of H_2O
639 concentration and temperatures: (a) from this study, compared to (b) Yoshino et al.
640 (2009) for polycrystalline hydrous olivine aggregates. The thick dashed lines indicate
641 the conditions at which proton conductivity and small polaron conductivity are equal as
642 a function of H_2O concentration, with small polaron conduction dominating at high T
643 and low [H_2O].

FIG. 1

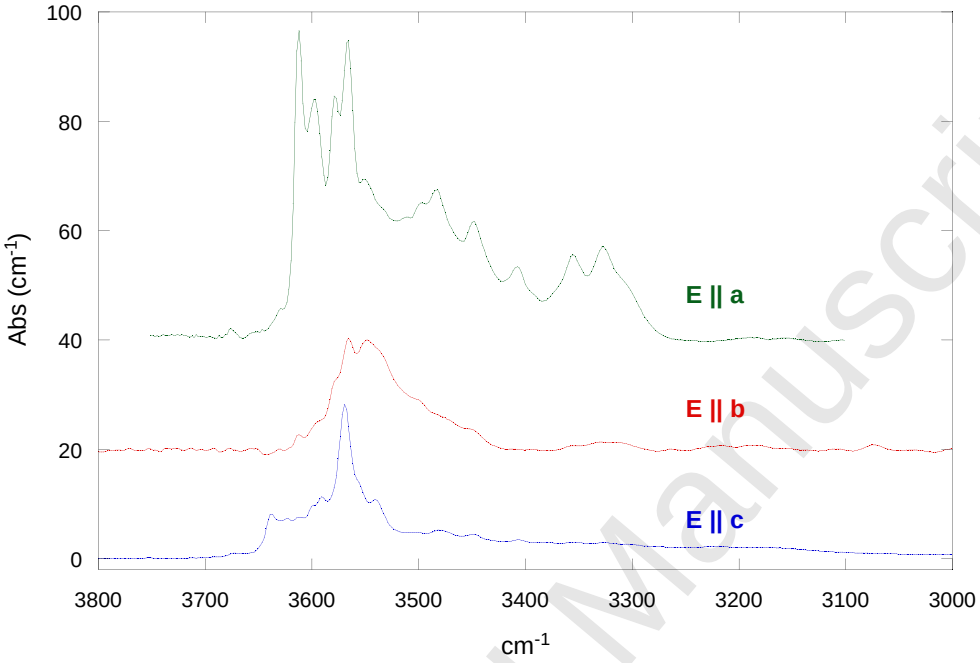

FIG. 2

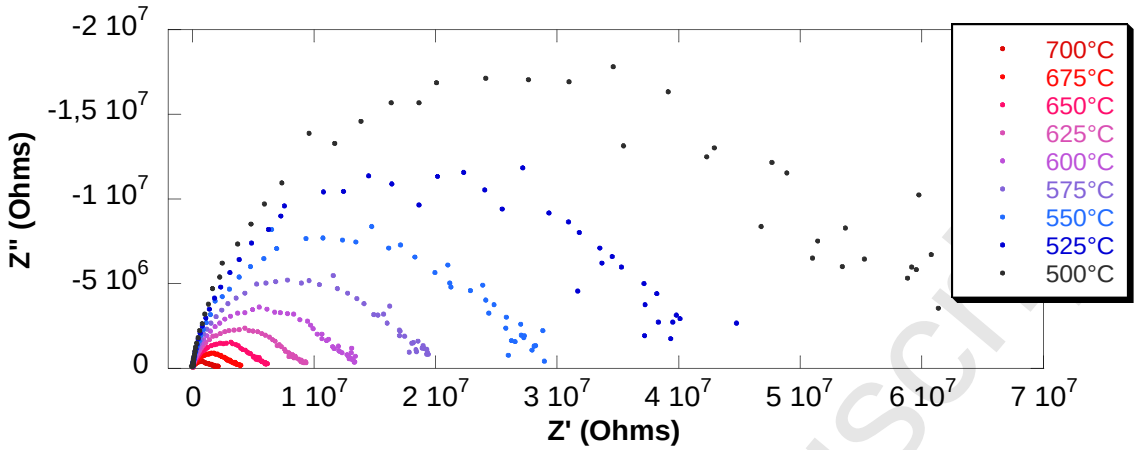

FIG. 3

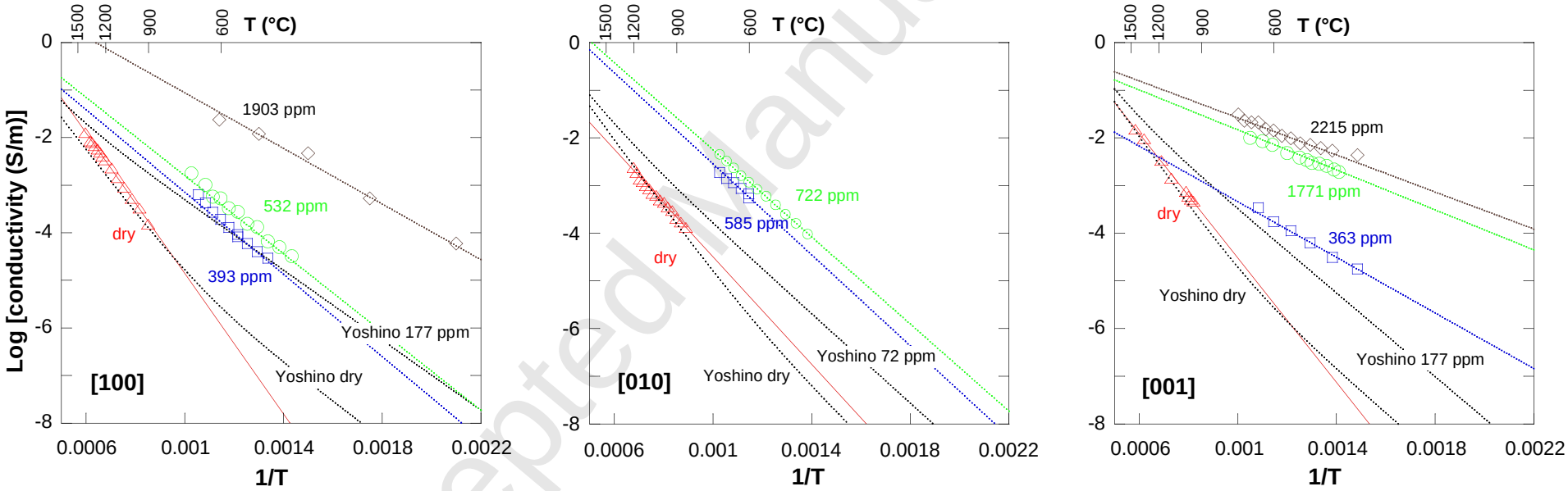

FIG. 4

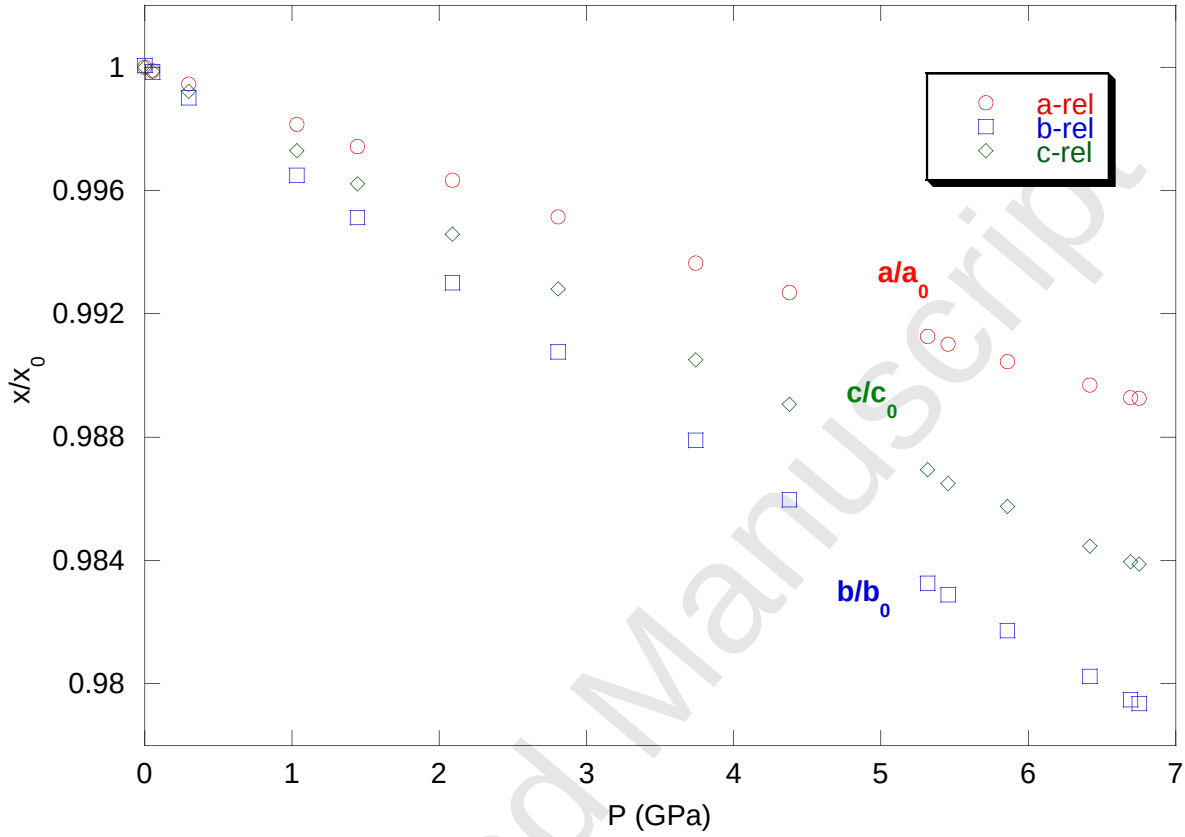

FIG. 5

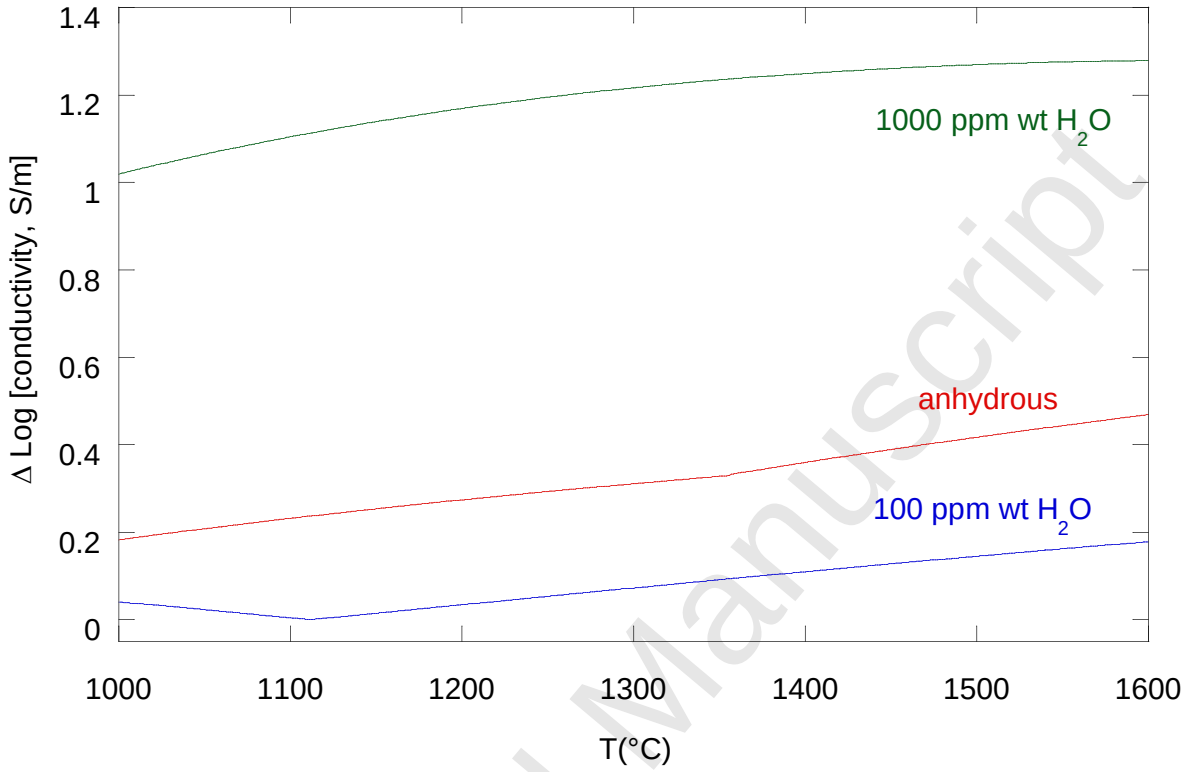

Fig. 6

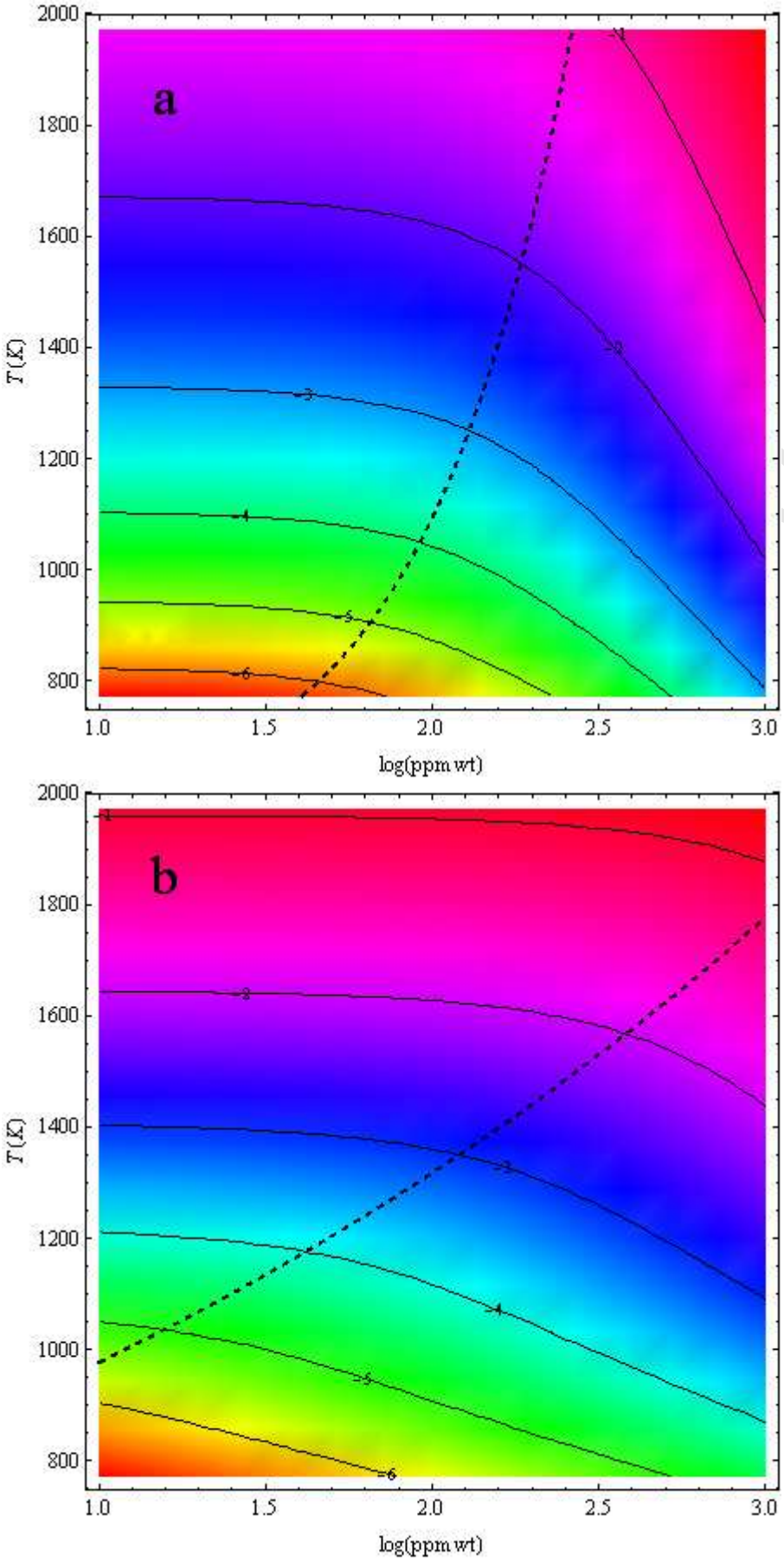

Table 1. Fitting parameters of Arrhenius equation (Eq. 1) to experimental data (8 GPa). Linear correlation coefficient R is also given to indicate goodness of fit. Standard error in H_2O analyses by FTIR is given in parentheses.

expt	orient.	[H_2O] wt. ppm	σ_o (S/m)	H (eV)	R
H2329	[100]	nom. dry	334	1.46	0.9992
H2474	[100]	393(71)	57.2	0.944	0.9952
H2473	[100]	532(85)	41.1	0.851	0.9958
H2320	[100]	1903(230)	48.1	0.555	0.9939
H2476	[010]	nom. dry	13.8	1.12	0.9964
H2480	[010]	585(62)	33.1	0.819	0.9883
H2477	[010]	722(65)	247	0.919	0.9996
H2328	[001]	nom. dry	99.0	1.29	0.9982
H2472	[001]	363(52)	0.802	0.628	0.9963
H2324	[001]	1771(220)	1.37	0.401	0.9962
S3740	[001]	2215(260)	1.70	0.340	0.9824
G.M. dry			77.0	1.29	
Yoshino	[100]	nom. dry		1.35	
Yoshino	[010]	nom. dry		1.42	
Yoshino	[001]	nom. dry		1.47	

Table 2. Unit-cell parameters at different pressures of forsterite studied in this work. Standard error in last digit shown in parentheses.

P (GPa)	*a* (Å)	*b* Å	*c* (Å)	V (Å^3)
0.00010(1)	4.7602(1)	10.2155(1)	5.9874(3)	291.15(1)
0.055(3)	4.7596(1)	10.2135(1)	5.9866(3)	291.02(1)
0.298(2)	4.7576(1)	10.2048(1)	5.9827(2)	290.46(1)
1.035(3)	4.7514(1)	10.1792(1)	5.9712(3)	288.80(1)
1.445(3)	4.7480(1)	10.1651(1)	5.9648(3)	287.88(1)
2.091(4)	4.7428(1)	10.1436(1)	5.9550(3)	286.49(2)
2.809(4)	4.7371(2)	10.1206(2)	5.9444(4)	284.99(2)
3.741(4)	4.7299(2)	10.0915(2)	5.9306(4)	283.08(2)
4.376(5)	4.7254(1)	10.0717(2)	5.9220(4)	281.85(2)
5.316(6)	4.7187(1)	10.0440(2)	5.9092(4)	280.06(2)
*5.454(7)	4.7174(1)	10.0402(3)	5.9065(7)	279.75(4)
5.859(6)	4.7147(1)	10.0284(2)	5.9021(6)	279.06(3)
6.417(7)	4.7111(1)	10.0131(3)	5.8944(8)	278.06(4)
6.696(6)	4.7092(3)	10.0054(4)	5.8914(9)	277.59(5)
6.750(7)	4.7091(5)	10.0042(6)	5.8909(14)	277.52(7)
Notes: *data measured during decompression				

Table 3. Best fit parameters for hydrous olivine conduction. Standard error shown in parentheses. Chi-squared values are also shown as an indication of goodness of fit.

$$\sigma = \sigma_0 C_W \exp\left(\frac{-H - \alpha C_W^{1/3}}{kT}\right)$$

orientation	σ_0	H(eV)	α	χ^2
100	3.86(1.36) x10^{-2}	1.26(0.04)	-5.49(0.20) x 10^{-2}	0.21
010	0.290(0.061)	1.50(0.05)	-6.64(0.50) x 10^{-2}	0.013
001	1.04(0.22) x 10^{-3}	0.812(0.016)	-3.27(0.07) x 10^{-2}	0.079

$$\sigma = \sigma_0 C_W^r \exp\left(\frac{-H}{kT}\right)$$ (from Wang et al., 2006)

orientation	σ_0	H(eV)	r	χ^2
100	3.53(3.72) x 10^{-10}	0.628(0.044)	3.55(0.20)	0.95
010	2.59(2.60) x 10^{-8}	0.911(0.014)	3.47(0.16)	0.010
001	1.70(1.03) x 10^{-9}	0.440(0.026)	2.53(0.06)	0.24